Original Research

Effect of Demineralized Bone Matrix, Bone Marrow Mesenchymal Stromal Cells, and Platelet-Rich Plasma on Bone Tunnel Healing After Anterior Cruciate Ligament Reconstruction

A Comparative Micro-Computed Tomography Study in a Tendon Allograft Sheep Model

Adam T. Hexter,*† MBBS, BSc, Aikaterina Karali,‡ PhD, Alex Kao,‡ PhD, Gianluca Tozzi,‡ PhD, Nima Heidari,§ MBBS, MSc, Aviva Petrie,‖ BSc, MSc, Ashleigh Boyd,† PhD, Deepak M. Kalaskar,† PhD, Catherine Pendegrass,† PhD, Scott Rodeo,¶ MD, Fares Haddad,# MBBS, MD(Res), and Gordon Blunn,** PhD

Investigation performed at University College London Institute of Orthopaedics and Musculoskeletal Sciences, Division of Surgery and Interventional Science, Royal National Orthopaedic Hospital, Brockley Hill, Stanmore, London

Background: The effect of demineralized bone matrix (DBM), bone marrow–derived mesenchymal stromal cells (BMSCs), and platelet-rich plasma (PRP) on bone tunnel healing in anterior cruciate ligament reconstruction (ACLR) has not been comparatively assessed.

Hypothesis: These orthobiologics would reduce tunnel widening, and the effects on tunnel diameter would be correlated with tunnel wall sclerosis.

Study Design: Controlled laboratory study.

Methods: A total of 20 sheep underwent unilateral ACLR using tendon allograft and outside-in interference screw fixation. The animals were randomized into 4 groups (n = 5 per group): Group 1 received 4mL of DBM paste, group 2 received 10 million BMSCs in fibrin sealant, group 3 received 12 mL of activated leukocyte-poor platelet-rich plasma, and group 4 (control) received no treatment. The sheep were euthanized after 12 weeks, and micro-computed tomography scans were performed. The femoral and tibial tunnels were divided into thirds (aperture, midportion, and exit), and the trabecular bone structure, bone mineral density (BMD), and tunnel diameter were measured. Tunnel sclerosis was defined by a higher bone volume in a 250-μm volume of interest compared with a 4-mm volume of interest surrounding the tunnel.

Results: Compared with the controls, the DBM group had a significantly higher bone volume fraction (bone volume/total volume [BV/TV]) (52.7% vs 31.8%; $P = .020$) and BMD (0.55 vs 0.47 g/cm^3; $P = .008$) at the femoral aperture and significantly higher BV/TV at femoral midportion (44.2% vs 32.9%; $P = .038$). There were no significant differences between the PRP and BMSC groups versus controls in terms of trabecular bone analysis or BMD. In the controls, widening at the femoral tunnel aperture was significantly greater than at the midportion (46.7 vs 41.7 mm^2; $P = .034$). Sclerosis of the tunnel was common and most often seen at the femoral aperture. In the midportion of the femoral tunnel, BV/TV ($r = 0.52$; $P = .019$) and trabecular number ($r_S = 0.50$; $P = .024$) were positively correlated with tunnel widening.

Conclusion: Only DBM led to a significant increase in bone volume, which was seen in the femoral tunnel aperture and midportion. No treatment significantly reduced bone tunnel widening. Tunnel sclerosis in the femoral tunnel midportion was correlated significantly with tunnel widening.

Clinical Relevance: DBM might have potential clinical use to enhance healing in the femoral tunnel after ACLR.

Keywords: anterior cruciate ligament (ACL) reconstruction; microcomputed tomography; biological modulation; demineralized bone matrix (DBM); bone marrow–derived mesenchymal stromal cell (BMSC); platelet-rich plasma (PRP)

The clinical outcome of anterior cruciate ligament (ACL) reconstruction (ACLR) relies on the integration of tendon grafts into the bone tunnel, termed *tendon-bone healing*.[30] Bone tunnel widening is a common finding of unclear clinical significance after ACLR,[44] which has been associated with sclerosis of the tunnel wall whereby there is greater bone formation and remodeling at the immediate tunnel interface than of the surrounding bone.[24] Bone tunnel healing varies depending on the position in the tunnel, with healing at the aperture (the intra-articular opening) reported to be lower than that at the midportion and exit (the segment farthest from the intra-articular space).[3] The propensity for tendon-bone healing depends on the graft; hamstring tendon grafts are associated with a higher incidence of biological failures[43] and greater tunnel widening,[46] while tendon allografts have the advantage of avoiding donor-site morbidity but have delayed graft healing compared with autografts.[38] Therefore, strategies to enhance bone tunnel healing might be particularly advantageous for allogenic-free tendon grafts. Orthobiologics such as the use of platelet-rich plasma (PRP), demineralized bone matrix (DBM), and cell therapy could potentially enhance bone tunnel healing. Biologic augmentation has been described as the "next frontier" in ACLR, but comparative orthobiologic studies in large animals are rare.[29] Achieving more robust graft incorporation in the bone tunnels may enable early and more aggressive rehabilitation after ACLR.

DBM is an osteoinductive biomaterial derived from acid extraction of cortical bone[40] and in small animals has been shown to enhance tendon-bone healing.[13,19] In small animals, bone marrow–derived mesenchymal stromal cells (BMSCs) enhance tendon-bone healing by restoring a direct-type insertion[12] and have been shown to reduce tunnel widening.[14] Current clinical and preclinical studies suggest that PRP does not enhance bone tunnel healing,[7] but relatively few studies have used intraosseous injection.[32] Compared with ACLR in human clinical practice, small animal models use more elastic fixation systems, such as tying sutures to screw posts that are not typically used in humans, and this is likely to influence tendon-bone healing.[31] Therefore, large animal models that use contemporary fixation methods are necessary to investigate whether orthobiologics may enhance tendon-bone healing.[9]

This study aimed to compare the effect of DBM, BMSCs, and PRP on bone tunnel healing in a translational tendon allograft ACLR model. We hypothesized that these agents would significantly enhance bone tunnel healing as measured via an increase in bone mineral density (BMD) and bone volume fraction (bone volume/total volume [BV/TV]), which would be associated with a reduction in tunnel widening. We also hypothesized that tunnel widening would be highest at the tunnel apertures and would be correlated with tunnel wall sclerosis.

METHODS

Study Design

The research was conducted in accordance with a project license protocol accepted under the UK Home Office Animals (Scientific Procedures) Act 1986. A total of 20 skeletally mature, full-mouthed, female lowland Mule sheep (age range, 2-3 years; weight range, 60-75 kg) were used to evaluate healing in a bone tunnel in a translational ACLR model. Unilateral ACLR was performed using a superficial digital flexor tendon (SDFT) allograft and outside-in interference screw fixation. Animals were randomized into 4 groups (n = 5 animals per group). Group 1 received 2 mL of allogeneic DBM paste into each bone tunnel (4 mL total). In group 2, 10 million allogeneic culture-expanded BMSCs in fibrin sealant (Baxter) were applied to the graft (2 million) and bone tunnels (4 million per tunnel). In group 3, we injected 12 mL of PRP into the graft (4 mL)

The Orthopaedic Journal of Sports Medicine, 9(9), 23259671211034166
DOI: 10.1177/23259671211034166

*Address correspondence to Adam T. Hexter, MBBS, BSc, University College London Institute of Orthopaedics and Musculoskeletal Sciences, Division of Surgery and Interventional Science, Royal National Orthopaedic Hospital, Brockley Hill, Stanmore, London HA7 4LP, UK (email: a.hexter@ucl.ac.uk).
†Division of Surgery and Interventional Science, University College London, London, UK.
‡Zeiss Global Centre, School of Mechanical and Design Engineering, University of Portsmouth, Portsmouth, UK.
§Royal London Hospital and Orthopaedic Specialists (OS), London, UK.
‖Eastman Dental Institute, University College London, London, UK.
¶Hospital of Special Surgery, New York, New York, USA.
#University College London Hospitals, London, UK.
**School of Pharmacy and Biomedical Sciences, University of Portsmouth, Portsmouth, UK.
Final revision submitted March 12, 2021; accepted April 29, 2021.
One or more of the authors has declared the following potential conflict of interest or source of funding: The PRP aspects of the study were funded by a research donation from the Biotechnology Institute and Sovereign Medical Ltd, received by A.T.H., N.H., and G.B. A.T.H. received funding from a Royal Free Charity Project Grant. S.R. has received research support from OREF, Toulmin Foundation, and Angiocrine Biosciences; consulting fees from Advance Medical and Flexion Therapeutic; nonconsulting fees from Smith & Nephew; honoraria from Fidia Pharma; and royalties from Zimmer Biomet; has stock/stock options in Ortho RTI; and is a paid associate editor for *The American Journal of Sports Medicine*. F.H. has received royalties and consulting/speaking fees from Smith & Nephew, Stryker, MatOrtho, and Corin. AOSSM checks author disclosures against the Open Payments Database (OPD). AOSSM has not conducted an independent investigation on the OPD and disclaims any liability or responsibility relating thereto.
Ethical approval was not sought for the present study.

and the bone tunnels (4 mL per tunnel). In group 4 (control), the animals received no treatment.

After 12 weeks, the animals were euthanized and microcomputed tomography (μCT) scans were undertaken. BV/TV, trabecular thickness (Tb.Th), trabecular separation (Tb.Sp), trabecular number (Tb.N), BMD, and bone tunnel widening were quantified. The femoral and tibial tunnels were divided into thirds (aperture, midportion, and exit), and 2 volumes of interest (VOIs) were analyzed. Tunnel sclerosis was defined as a higher bone volume in a 250-μm VOI compared with a 4-mm VOI surrounding the tunnel. To assess the relationship between bone volume and remodeling at the immediate tunnel interface and tunnel diameter, correlations between trabecular microarchitecture in the 4-mm VOI and bone tunnel widening were examined.

DBM Paste Manufacture

Tibiae were harvested from the sheep. The soft tissues were stripped, the epiphyses were removed, and the diaphyseal bone region was cut into longitudinal strips (Exact). The strips were demineralized in 0.6-N hydrochloric acid for 5 days, and demineralization was confirmed via radiographs (300 s, 30 kV; Faxitron Corp). The strips were washed in phosphate-buffered saline and lyophilized (BOC-Edwards). Powdered DBM was made from the strips in a cryogenic grinding mill (6770 Freezer/Mill; SEPX SamplePrep). DBM powder was added to 100% glycerol (Sigma-Aldrich) in a 1:1 volume ratio that formed a paste, which was sterilized via gamma irradiation at a dose of 25 kGy (Isotron).

BMSC Harvest and Culture

Bone marrow was aspirated from a 2-year-old sheep (weight, 65 kg) under general anesthesia. We aspirated 10 mL of bone marrow (2 × 5 mL from different locations) from the posterior iliac crest into a 20-mL sterile polypropylene tube containing 10,000 IU of preservative-free heparin sodium (Wockhardt UK Ltd). The aspirate was combined with standard growth media, which was high glucose Dulbecco's modified Eagle medium (Invitrogen), 10% fetal calf serum (ThermoFisher), and 1% penicillin-streptomycin (ThermoFisher). The aspirate was plated directly onto T-150 culture flasks and cultured at 37°C in a 5% CO_2 incubator. After 72 hours, the flask contents were discarded and washed with phosphate-buffered saline to remove nonadherent cells, and fresh growth medium was added to supplement the cells that had attached to the flask. When 90% confluent, the cells were detached using 0.25% trypsin-EDTA (Gibco). The BMSCs were subcultured, and the growth medium was changed every 3 days. The 10 million allogenic cells from passage 3 were used in the surgical procedures to provide approximately 2 million cells in the graft and 4 million cells per bone tunnel.

PRP Preparation

PRP was prepared using the Endoret (plasma rich in growth factors) technology (BTI System IV/V; BTI Biotechnology Institute) using a 2-step centrifugation process. Peripheral venous blood (72 mL) was taken from the jugular vein into eight 9-mL tubes containing 3.8% (wt/vol) sodium citrate. The tubes were centrifuged twice for 8 minutes at 580*g* (1902 rpm) at room temperature (BTI System II; BTI Biotechnology Institute). The 2 mL of plasma located immediately above the sedimented erythrocytes and the buffy coat layer containing leukocytes were collected, giving a total PRP volume of 16 mL per animal. The plasma fraction was drawn up into 10-mL syringes and activated by adding calcium chloride (10% wt/vol), which produced a gel within 5 minutes that was injected into the tunnel. The time between venipuncture, PRP processing, activation, and delivery was approximately 30 minutes including the 16 minutes of centrifugation. The whole blood and PRP were stored at room temperature and only stored in the dark when inside the centrifuge. When using sheep blood, the PRP fraction generated using this technique has been shown to be enriched in platelets and reduced in leukocytes.[33]

SDFT Allograft Preparation

A posterolateral approach was used to expose the Achilles tendon, and the SDFT (approximately 80-90 mm in length and 7.5-8 mm in diameter) was harvested. The grafts were individually wrapped in isotonic saline-soaked gauze before being sterilized via gamma irradiation at a dose of 25 kGy (Isotron). The samples were stored at –20°C and thawed at room temperature 30 minutes before the surgical procedure. Both ends of the graft were prepared via a whipstitch using No. 2 Ethibond (Ethicon Inc).

Perioperative Anesthesia

Topical analgesic patches (75 mg of fentanyl) were administered 12 hours before surgery and for 60 hours after surgery. Anesthesia was intravenously induced using a combination of ketamine (100 mg/mL) and midazolam (5 mg/mL). Anesthesia was maintained using isoflurane in induction and sevoflurane in the operating theater vaporized in a mixture of oxygen and medical grade air (clean air at standard temperature and pressure). During surgery, antibiotic injection (penicillin-streptomycin) was administered, and further injections were given postoperatively to provide antibiotic cover until day 3.

Surgical Technique

The right hind limb was shaved, prepared, and draped. The stifle joint was exposed via a medial arthrotomy, and with knee extended, the patella dislocated laterally (Figure 1). In full flexion, the fat pad was resected, and the ACL was sharply excised, leaving no remnant tissue. Bone tunnels (7.8 mm diameter) were drilled using an inside-out technique. First, in deep flexion, the femoral tunnel was drilled from the center of the femoral ACL footprint to the lateral femoral condyle. Second, the tibial bone tunnel was drilled from the center of the tibial ACL to the anteromedial tibia 10 mm medial and 10 mm distal to the tibial tuberosity. The femoral and tibial tunnel lengths were approximately 24 to 26 and 30 to 32 mm, respectively. The SDFT was passed

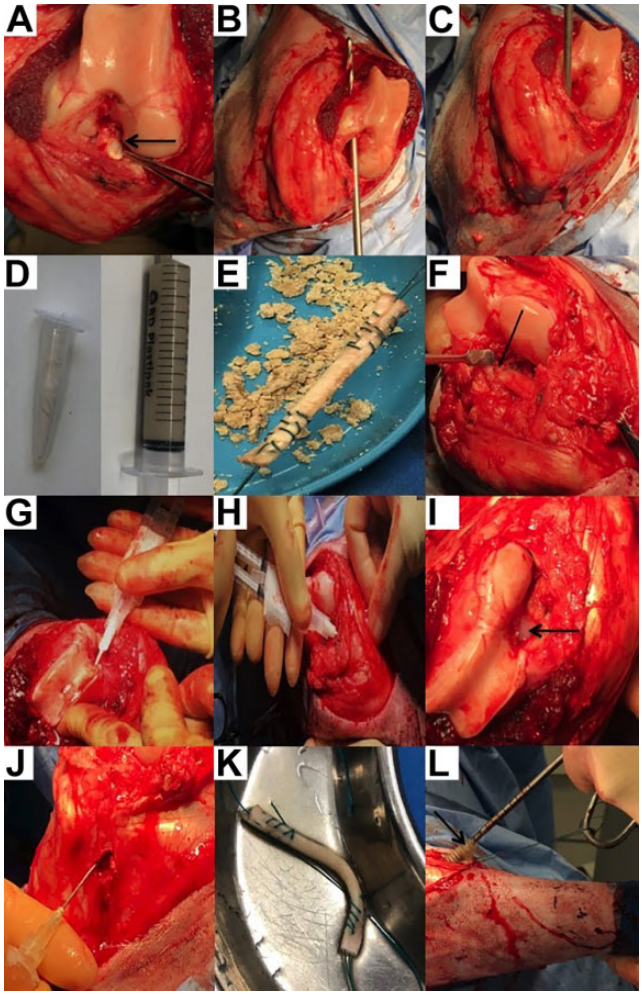

Figure 1. Surgical technique. (A) Ovine ACL (arrow). (B) Femoral tunnel. (C) Tibial tunnel. (D) DBM powder and paste. (E) SDFT graft rubbed in DBM paste. (F) DBM at femoral aperture (arrow). (G) BMSCs injected into femur. (H) BMSCs injected into tibia. (I) Fibrin glue at femoral aperture (arrow). (J) Intraosseous injection of PRP into tibia. (K) SDFT graft soaking in PRP. (L) Insertion of tibial screw, which is covered in PRP clot (arrow). ACL, anterior cruciate ligament; BMSC, bone marrow–derived mesenchymal stromal cell; DBM, demineralized bone matrix; PRP, platelet-rich plasma; SDFT, superficial digital flexor tendon.

into the bone tunnels and fixed using an outside-in interference screw technique. First, the femoral fixation was achieved using an 8 × 20–mm Biosure PK interference screw (Smith & Nephew Endoscopy). Then, tibial fixation was achieved with the stifle joint in extension using an 8 × 25–mm Biosure interference screw (Smith & Nephew Endoscopy) at a tension of 40 N, which has been used in previous ovine ACLR studies.[17,18,45] The excess graft length was cut to be flush with the bone tunnel exit. The median (interquartile range) length of the femoral tunnel was 23.5 mm (21.50-24.25 mm) versus 29.5 mm (27.75-32.25 mm) for the tibial tunnel.

In group 1, we introduced 2 mL of DBM paste into each bone tunnel (4 mL in total); 1 mL was applied before the graft was inserted, and a spatula was used to press the DBM into the bony trabeculae in the vicinity of the bone tunnel. After the graft was in position in the bone tunnels, 1 mL of DBM was applied around the graft in the tunnel.

In group 2, at 1 hour before surgery, the MSCs were loaded into 2 mL of frozen prefilled 2-component fibrin sealant (Baxter). One component (1 mL) contained fibrinogen, and the other component (1 mL) contained thrombin; 10 million BMSCs were added to the thrombin component. For intraoperative application, the 2 thrombin and fibrinogen components were mixed in a 2-way cannula. Then, 0.8 mL of fibrin sealant (approximately 4 million BMSCs) was added to each bone tunnel, and 0.4 mL of fibrin sealant (approximately 2 million BMSCs) covered the intra-articular graft (Figure 1, G-H).

In group 3, the graft was infiltrated with 4 mL of activated PRP parallel to its fibers along the length of the graft at varied depths. The graft was left in a kidney dish soaking in activated PRP until implantation. The interference screws were opened and immersed in 4 mL of activated PRP in a kidney dish until implantation. After 5 minutes, the clotted PRP was adherent to the screw (Figure 1L). Before inserting the graft, the spongy bone in the tunnels was infiltrated to expose the bone in contact with the graft to PRP. Using a 19-gauge needle, 1 mL was injected at 4 intervals along the tunnel wall. In total, 4 mL were injected in the femoral tunnel, and 4 mL were injected in the tibial tunnel.

In group 4, the ACLR procedure was performed in the same way but without application of DBM, BMSCs, or PRP.

After graft insertion, the stifle joint was taken through 10 full ranges of motion, and the incision was closed in layers beginning with the deep fascia. A simple adhesive dressing plus cotton wool and bandage was applied and removed 48 hours after surgery. The animals were allowed full weightbearing immediately, with no limitation to range of motion. In the first week after surgery, animals freely mobilized in individual pens with no exercise protocol, and pain was controlled using multimodal postoperative analgesia. Thereafter, the animals were housed in a large group, provided with a constant supply of natural light, and fed on hay and supplementary minerals. Animals were assessed for complications such as infection daily. The animals were euthanized at 12 weeks postoperatively.

μCT Analysis

To determine mineralization and new bone formation at the graft-bone interface, the femur-SDFT-tibia complexes were analyzed using μCT. Using a saw, the femur was cut proximal to the femoral tunnel, and the tibia was cut distal to the tibial tunnel. The specimens were fixed in 10% buffered formalin at room temperature for 7 days and then transferred to 50% ethanol. For scanning, specimens were stored in 50% ethanol in a sealed plastic container. The μCT scans were performed using an Xradia 520 Versa (Carl Zeiss Microscopy) at 70 kVp (peak energy), 85.4 μA, 0.4-second exposure, 1601 projections, and 5 frames per projection image captured on a flat panel detector to achieve a final

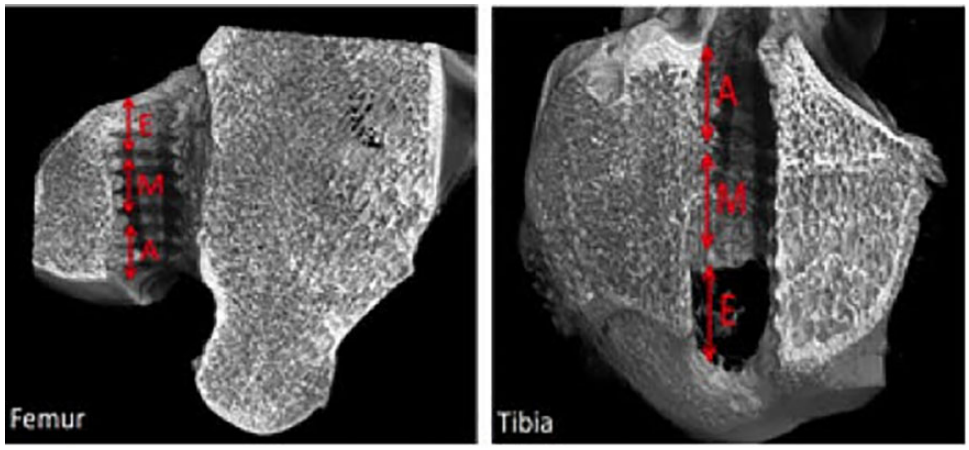

Figure 2. μCT images showing the segments of the femoral (left) and tibial (right) tunnel. A, aperture; M, middle; E, exit.

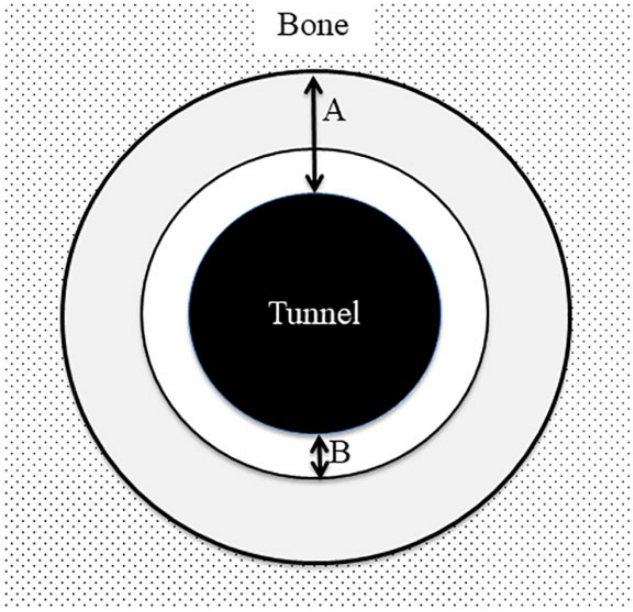

Figure 3. Schematic (not to scale) showing the volumes of interest (VOIs): 4-mm VOI (*A*) and 250-μm VOI (*B*).

voxel size of 40.25 μm. The specimens were imaged in 2 sections because of their size (ie, top and bottom), and virtual stitching, based on feature registration, was executed to obtain the whole volume after reconstruction (filtered back projection) and then exported to 16-bit grayscale images.

Two 32-mm calibration phantoms (calcium hydroxylapatite [CaHA] densities, 0.25 and 75 g/cm^3; Bruker) were scanned under the same conditions. The phantom scale was applied during the reconstruction of the data sets in order to tune the contrast of the images according to the phantom readings. After scanning, images were segmented using CT-Analyzer software Version 1.15 (Bruker). The bone tunnel was reconstructed parallel to the longitudinal axis of the tunnel in both the sagittal and the coronal planes. The bone tunnels were divided into equal thirds: the segment closest to the intra-articular space was called the aperture, the middle segment was called the midportion, and the segment closest to the extra-articular opening was called the exit (Figure 2). Each segment was individually analyzed for trabecular bone structure, BMD, and tunnel widening.

Trabecular Bone Analysis

Analysis of the microstructure of the trabecular bone surrounding the bone tunnel was performed using CT-Analyzer software. Two VOIs were analyzed and chosen based on preliminary scans (Figure 3). The 4 mm of bone surrounding the bone tunnel was used to measure the bone in general around the tunnel, while a smaller VOI 250 μm directly adjacent to the tunnel margin was used to analyze bone healing at the immediate tunnel interface, where sclerosis would most likely be seen. The VOI analysis only included the bone surrounding the bone tunnel, without including the actual bone tunnel itself. The analysis included the BV/TV, Tb.Th, Tb.Sp, and Tb.N, which were calculated for the 2 cylindrical VOIs in the tunnel segment.

Tunnel Wall Sclerosis

Tunnel wall sclerosis was characterized by increased bone formation and remodeling at the immediate tunnel interface compared with the surrounding bone. Increased bone formation was indicated by an increase in BV/TV, Tb.Th, and Tb.N and reduction in Tb.Sp. Therefore, tunnel sclerosis was defined by increased BV/TV, Tb.Th, and Tb.N and reduced Tb.Sp in the 250-μm VOI relative to the 4-mm VOI.

Bone Mineral Density

BMD has previously been considered to be indicative of the quality of healing between tendon and bone.[19] The same 2 VOIs were analyzed (4 mm and 250 μm). BMD was measured using grayscale via ImageJ software Version 1.52s (US National Institutes of Health). The mean grayscale

values for the VOI were determined. A calibration curve was generated to calculate BMD using the CaHA phantoms as a reference.

Bone Tunnel Widening

The cross-sectional area of the bone tunnel in the perpendicular plane of the femoral and tibial tunnel longitudinal axes were determined using CT-Analyzer software. A software tool for calculating areas that defined the tunnel wall via a polygonal figure was used. Tunnel widening was defined by the difference between the cross-sectional area of the drill bit and the area measured on μCT. Percentage tunnel expansion was calculated as net change in cross-sectional area from the time of surgery to 12 weeks. The extent of widening was classified based on percentage increase on the initial tunnel diameter based on a previous classification system[24]: grade 0 (no widening) indicated <10% widening observed compared with the drill bit measurement; grade 1 (mild), 10% to 25% widening; grade 2 (moderate), 25% to 50% widening; grade 3 (severe), 50% to 100% widening; and grade 4 (very severe), >100% widening. This was calculated by dividing the amount of tunnel widening by the original tunnel (drill bit) diameter.

Radiographic Assessment of Bone Tunnel Appearance

Lateral radiographs of the stifle joints were taken after 12 weeks. Signs of bone tunnel widening and sclerosis were examined qualitatively by 2 independent and blinded radiologists.

Statistical Analysis

The data did not follow a normal distribution and therefore were summarized by using the median and interquartile range. Box-and-whisker plots were used to express these values. The nonparametric Kruskal-Wallis 1-way analysis of variance was used to compare the distributions of the trabecular bone analysis, BMD, and tunnel diameters among groups for each tunnel segment. If the Kruskal-Wallis test produced a significant result, post hoc pairwise

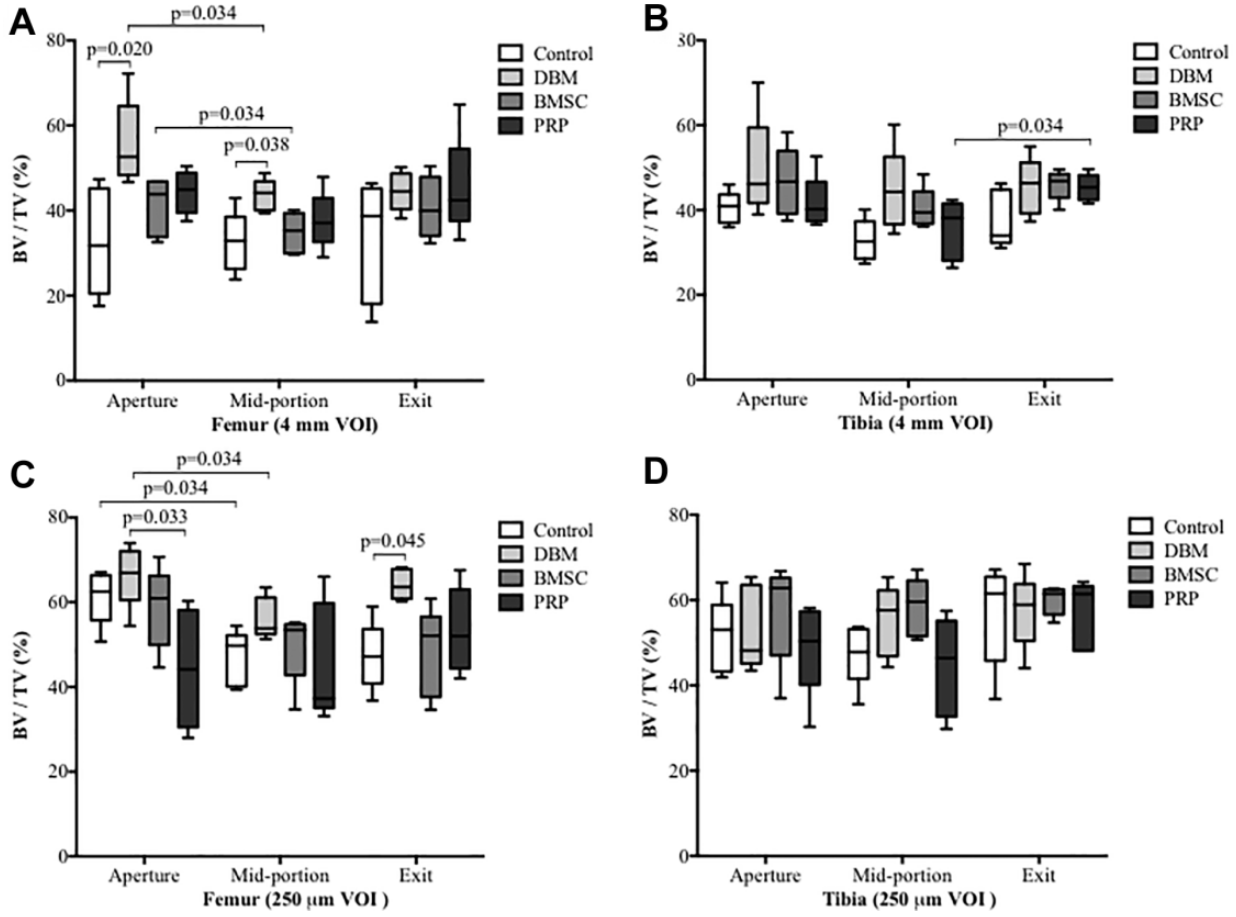

Figure 4. Box-and-whisker plots showing the bone volume/total volume (BV/TV) by treatment group in each bone tunnel segment and region volume of interest (VOI). (A) Femoral 4-mm VOI, (B) tibial 4-mm VOI, (C) femoral 250-μm VOI, and (D) tibial 250-μm VOI (n = 5 in each group). Bonferroni-adjusted *P* values from the Mann-Whitney *U* test. BMSC, bone marrow–derived mesenchymal stromal cell; DBM, demineralized bone matrix; PRP, platelet-rich plasma.

comparisons of groups were performed using the Mann-Whitney *U* test with the Bonferroni correction to adjust the *P* values for multiple testing. Comparison among different segments of the tunnel within the same group was performed using the nonparametric Friedman 2-way analysis of variance, and when significant differences were seen, comparisons using the Wilcoxon signed rank test with the Bonferroni adjustment to the *P* values were used to make pairwise comparisons. The Mann-Whitney *U* test was used to compare 2 different VOIs for each tunnel segment and to compare the femoral tunnel and tibial tunnel for each tunnel segment. Correlations among the tunnel cross-sectional area, tunnel sclerosis, and graft calcification were examined using the Spearman rank correlation coefficient (r_S). IBM SPSS Statistics for Windows Version 26 (IBM Corp) was used for statistical analysis. The level of statistical significance was set at $P = .05$.

RESULTS

Postoperative Course

There were no complications that led to any animals being excluded from the study.

Trabecular Bone Analysis

Only significant differences are highlighted in this section. The complete data set for the trabecular bone analysis are shown in Appendix Tables A1 and A2.

Bone Volume Fraction

Comparison Among Treatment Groups. In the 4-mm VOI, the DBM group had a significantly higher median BV/TV at the femoral aperture ($P = .020$) and the femoral tunnel in the midportion ($P = .038$) when compared with the control group (Figure 4A). In the 250-μm VOI, the femoral aperture of the DBM group had a significantly higher median BV/TV than did the PRP group ($P = .033$). In the 250-μm VOI at the femoral exit, the DBM group had a significantly higher median BV/TV than did the control group ($P = .045$) (Figure 4C).

Spatial Changes Within the Bone Tunnels. In the 4-mm VOI, in the DBM and BMSC groups, the median BV/TV was significantly higher at the femoral aperture compared with the femoral midportion (both $P = .034$) (Figure 4A). In the 4-mm VOI in the PRP group, the median BV/TV was significantly higher at the tibial exit compared with that at the tibial midportion ($P = .034$)

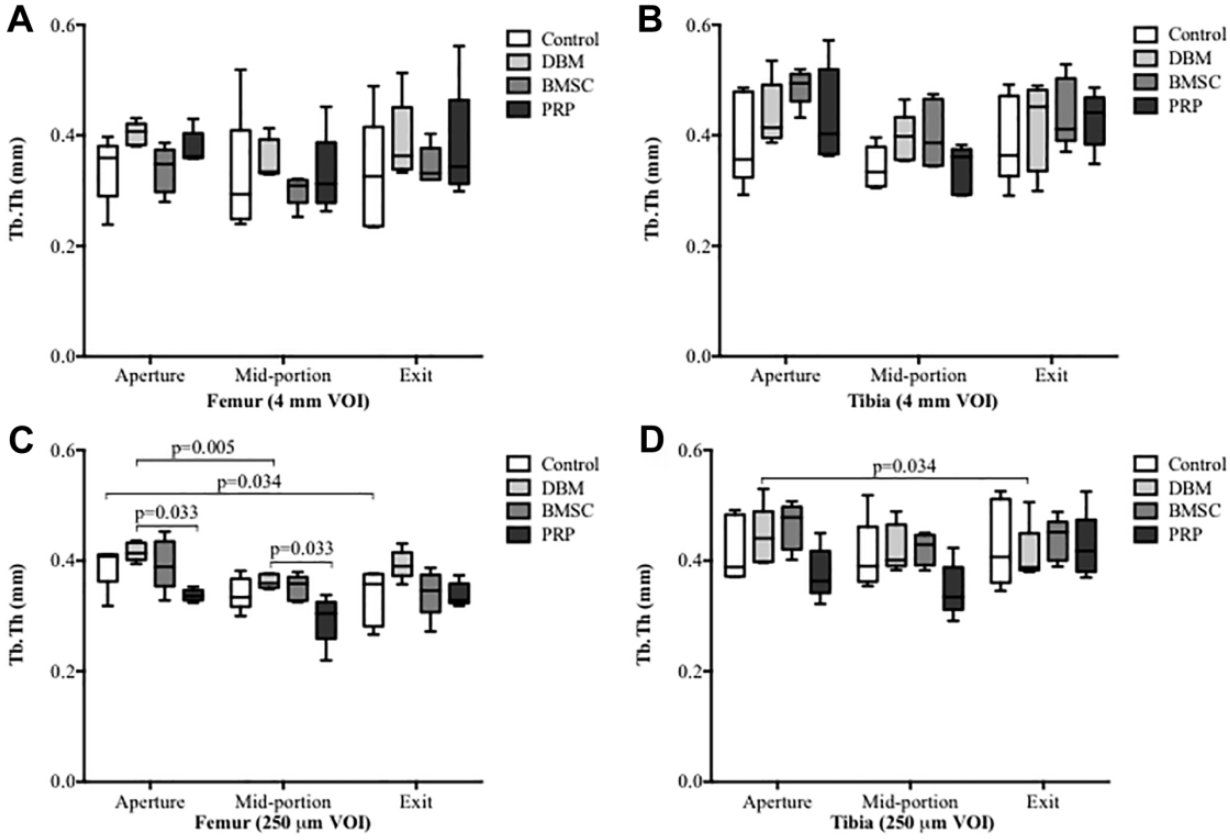

Figure 5. Box-and-whisker plots showing the trabecular thickness (Tb.Th) by treatment group in each bone tunnel and volume of interest (VOI). (A) Femoral 4-mm VOI, (B) tibial 4-mm VOI, (C) femoral 250-μm VOI, and (D) tibial 250-μm VOI (n = 5 in each group). BMSC, bone marrow–derived mesenchymal stromal cell; DBM, demineralized bone matrix; PRP, platelet-rich plasma.

(Figure 4B). In the 250-μm VOI in the control and DBM groups, the median BV/TV was significantly higher at the femoral aperture compared with that at the femoral midportion (both $P = .034$) (Figure 4C).

Comparison Between the 2 VOIs. In the control group, the median BV/TV was significantly higher in the 250-μm versus the 4-mm VOI at the femoral aperture ($P = .008$), femoral midportion ($P = .032$), tibial aperture ($P = .032$), tibial midportion ($P = .016$), and tibial exit ($P = .032$). In the DBM group, the median BV/TV was significantly higher in the 250-μm versus the 4-mm VOI at the femoral midportion ($P = .008$) and femoral exit ($P = .008$). In the BMSC group, the median BV/TV was significantly higher in the 250-μm versus the 4-mm VOI at the femoral aperture ($P = .032$) and tibial midportion ($P = .008$). In the PRP group, the median BV/TV was significantly higher in the 250-μm versus the 4-mm VOI at the tibial exit only ($P = .032$).

Trabecular Thickness

Comparison Among Treatment Groups. No significant differences were seen among treatment group distributions in the 4-mm VOI region (Figure 5, A and B), but closer to the tunnel within the 250-μm VOI, the DBM group had a significantly greater median Tb.Th at the femoral aperture and femoral midportion (both $P = .033$) when compared with the PRP group (Figure 5C).

Spatial Changes Within the Bone Tunnels. Analysis in the 250-μm VOI around the femoral tunnel in the control group showed that Tb.Th was significantly greater at the aperture compared with the exit ($P = .034$) (Figure 5C). In the DBM group, the Tb.Th was significantly greater at the femoral aperture compared with the midportion ($P = .005$), and in the tibial tunnel, the Tb.Th was significantly greater at the aperture compared with the exit ($P = .034$) (Figure 5, C and D).

Comparison Between Bone Tunnels. In the BMSC group, the median Tb.Th was significantly greater for the femoral midportion compared with the tibial midportion for the 4-mm VOI ($P = .008$) and the femoral exit compared with the tibial exit for the 4-mm VOI ($P = .016$).

Comparison Between the 2 VOIs. In the BMSC group, the Tb.Th was significantly greater on average in the 250-μm VOI compared with the 4-mm VOI at the femoral midportion only ($P = .008$). In the PRP group, the Tb.Th was significantly greater on average in the 250-μm VOI compared with the 4-mm VOI at the femoral aperture only ($P = .008$).

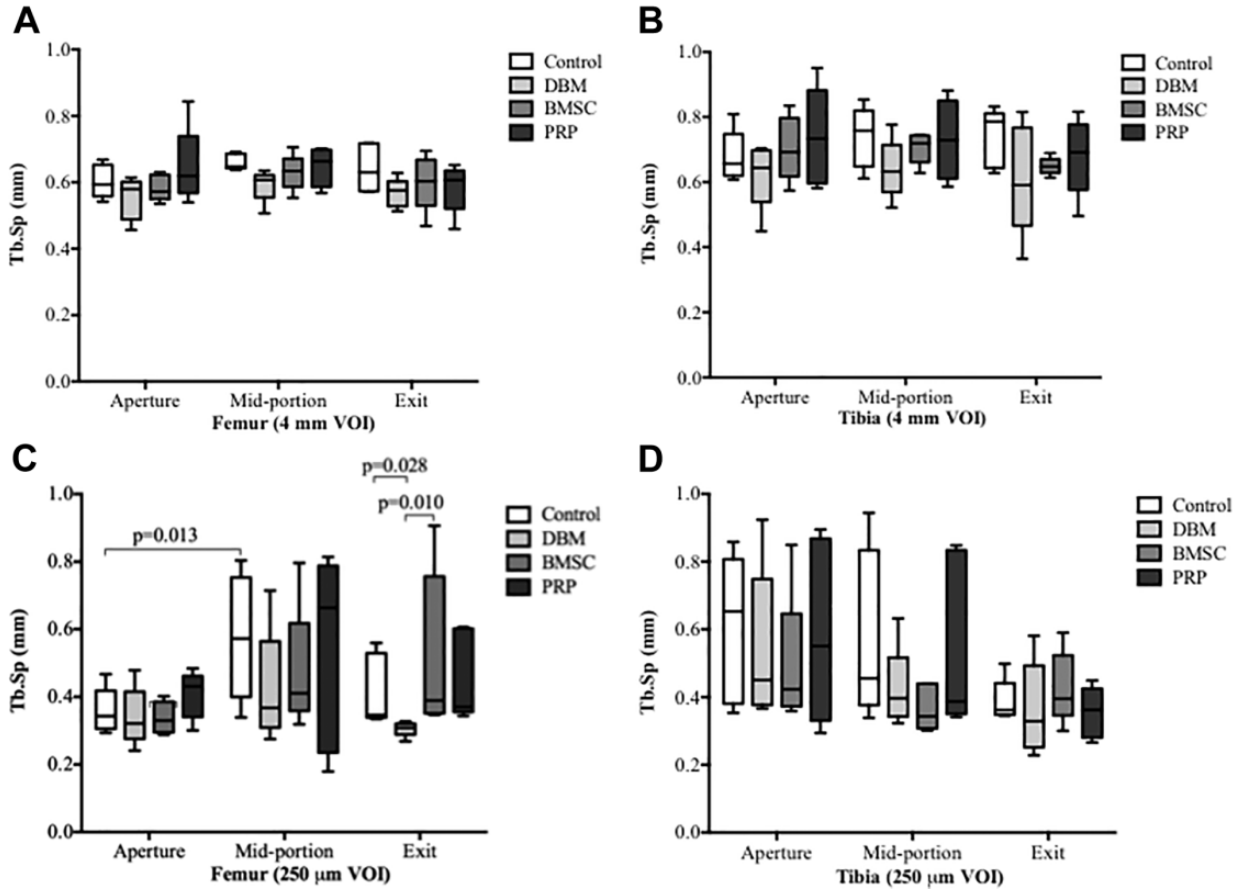

Figure 6. Box-and-whisker plots showing the trabecular separation (Tb.Sp) by treatment group in each bone tunnel and volume of interest (VOI). (A) Femoral 4-mm VOI, (B) tibial 4-mm VOI, (C) femoral 250-μm VOI, and (D) tibial 250-μm VOI (n = 5 in each group). BMSC, bone marrow–derived mesenchymal stromal cell; DBM, demineralized bone matrix; PRP, platelet-rich plasma.

Trabecular Separation

Comparison Among Treatment Groups. In terms of the 250-μm VOI, there was a significantly smaller median Tb.Sp at the femoral exit in the DBM group compared with the BMSC group ($P = .010$) and the control group ($P = .028$) (Figure 6).

Spatial Changes Within the Bone Tunnels. In terms of the 250-μm VOI, in the control group, the median Tb.Sp was significantly smaller at the femoral aperture compared with the femoral midportion ($P = .013$) (Figure 6).

Comparison Between Bone Tunnels. In terms of the 4-mm VOI, in the BMSC group, the median Tb.Sp was significantly larger in the tibial aperture compared with the femoral aperture ($P = .032$).

Comparison Between the 2 VOIs. In the control group, the Tb.Sp was significantly smaller on average in the 250-μm versus the 4-mm VOI at the femoral aperture ($P = .008$), femoral exit ($P = .008$), and tibial exit ($P = .008$). In the DBM group, the Tb.Sp was significantly smaller on average in the 250-μm versus the 4-mm VOI at the femoral aperture ($P = .016$), femoral exit ($P = .008$), and tibial midportion ($P = .040$). In the BMSC group, the median Tb.Sp was significantly smaller in the 250-μm versus the 4-mm VOI at the femoral aperture ($P = .008$), tibial midportion ($P = .008$), and tibial exit ($P = .008$). In the PRP group, the median Tb.Sp was significantly smaller in the 250-μm versus the 4-mm VOI at the femoral aperture ($P = .008$) and tibial exit ($P = .008$).

Trabecular Number

Comparison Between Bone Tunnels. In the BMSC group, the Tb.N was significantly larger on average in the femoral aperture compared with the tibial aperture for the 4-mm VOI ($P = .016$). In the PRP group, the Tb.N was significantly larger on average in the femoral aperture compared with the tibial aperture for the 4-mm VOI ($P = .016$). No differences were found among groups (Figure 7).

Comparison Between the 2 VOIs. In the control group, the median Tb.N was significantly larger in the 250-μm versus the 4-mm VOI at the femoral aperture ($P = .008$), femoral midportion ($P = .016$), and tibial exit ($P = .016$). In the DBM group, the median Tb.N was significantly larger in the 250-μm versus the 4-mm VOI at the femoral midportion ($P = .016$) and femoral exit ($P = .008$). In the BMSC group, the median Tb.N was significantly larger in the 250-μm versus the 4-mm VOI at the femoral aperture ($P = .008$), tibial midportion ($P = .008$), and tibial exit ($P = .008$). In the PRP group, the median Tb.N was significantly higher in the 250-μm versus the 4-mm VOI at the femoral exit ($P = .024$) and tibial exit ($P = .008$).

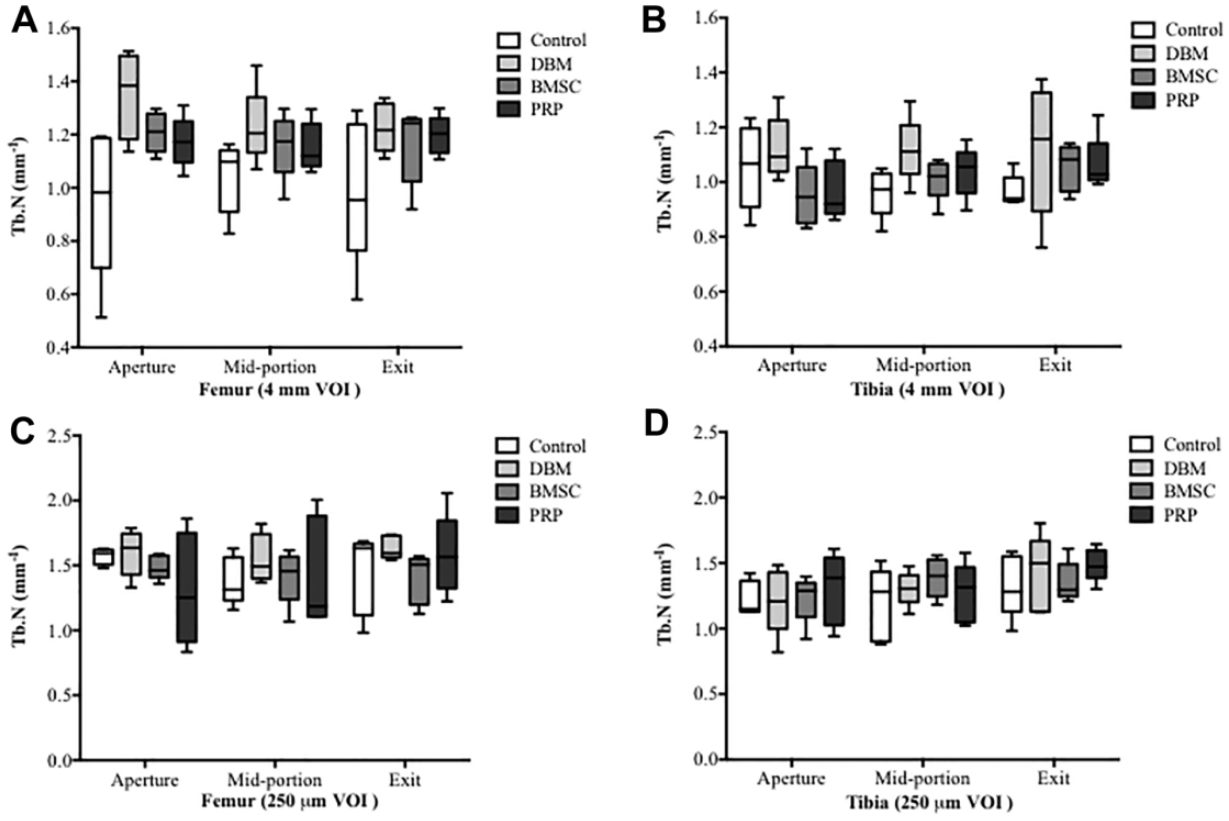

Figure 7. Box-and-whisker plots showing the trabecular number (Tb.N) by treatment group in each bone tunnel and volume of interest (VOI). (A) Femoral 4-mm VOI, (B) tibial 4-mm VOI, (C) femoral 250-μm VOI, and (D) tibial 250-μm VOI (n = 5 in each group). BMSC, bone marrow–derived mesenchymal stromal cell; DBM, demineralized bone matrix; PRP, platelet-rich plasma.

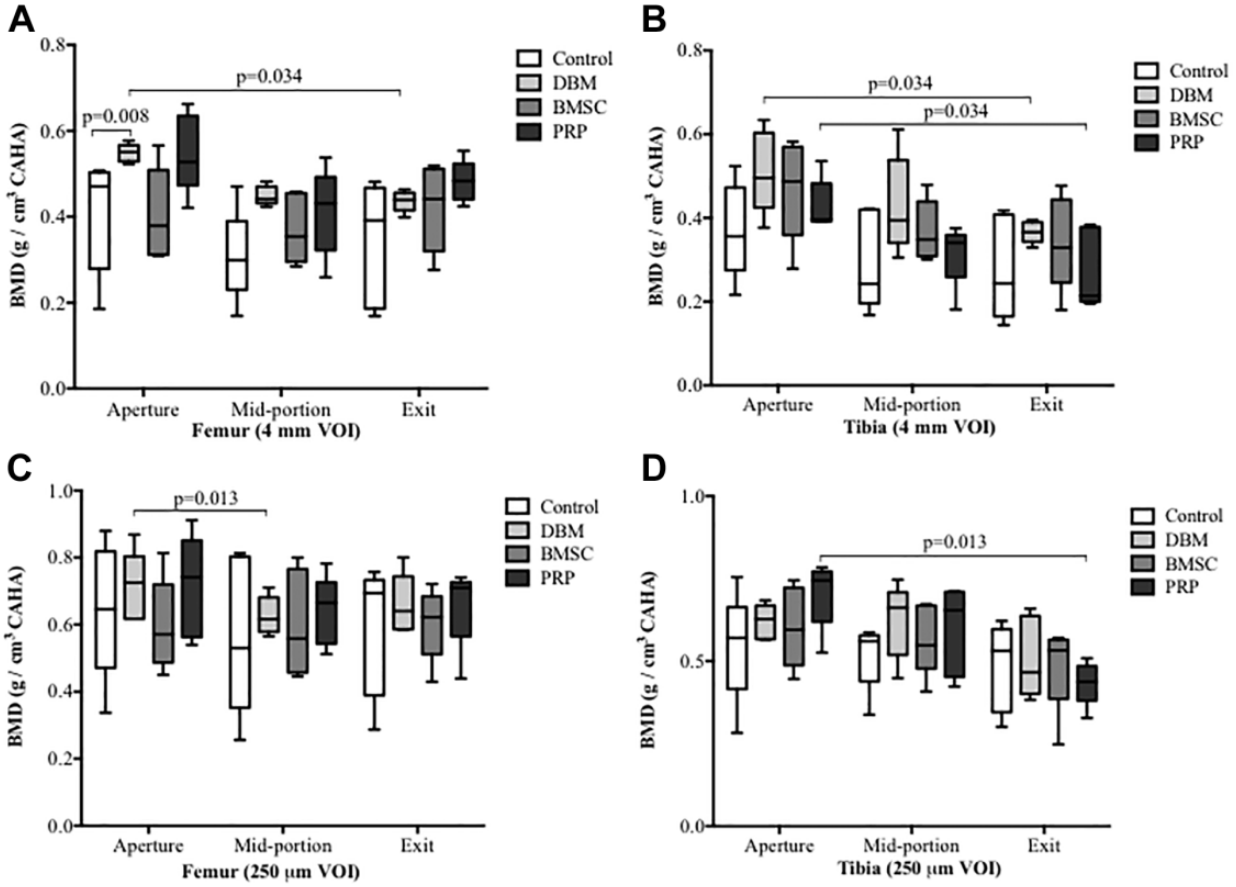

Figure 8. Box-and-whisker plots showing bone mineral density (BMD) by treatment group in each bone tunnel and volume of interest (VOI). (A) Femoral 4-mm VOI, (B) tibial 4-mm VOI, (C) femoral 250-μm VOI, and (D) tibial 250-μm VOI (n = 5 in each group). BMSC, bone marrow–derived mesenchymal stromal cell; CaHA, calcium hydroxylapatite; DBM, demineralized bone matrix; PRP, platelet-rich plasma.

Bone Mineral Density

The BMD values for the 4-mm and 250-μm VOIs are shown in Table A3.

Comparison Among Treatment Groups. In the 4-mm VOI, the DBM group had a significantly higher BMD on average at the femoral aperture than did the control group ($P = .008$). The mean average value for the femoral tunnel in the DBM group was significantly higher on average than that of the control group ($P = .032$) (Figure 8A).

Comparison Within Treatment Groups in Same Bone Tunnel. In the 4-mm VOI, in the DBM group, the median BMD was significantly higher at the aperture compared with the exit in the femoral tunnel ($P = .034$) and tibial tunnel ($P = .034$) (Figure 8, A and B). In the 4-mm VOI, in the PRP group, the median BMD was significantly higher at the aperture compared with the exit in the tibial tunnel ($P = .034$). In the 250-μm VOI, in the DBM group in the femoral tunnel, the median BMD was significantly higher at the aperture compared with the midportion ($P = .013$). In the 250-μm VOI, in the PRP group, the median BMD was significantly higher at the aperture compared with the exit in the tibial tunnel ($P = .013$) (Figure 8, C and D).

Comparison Between Bone Tunnels. In the DBM group, the median BMD was significantly higher in the femoral exit compared with the tibial exit for the 4-mm VOI ($P = .008$). In the PRP group, the median BMD was significantly higher in the femoral exit compared with the tibial exit for the 4-mm VOI ($P = .008$), and the overall mean for the femur was significantly higher on average than that for the tibia ($P = .016$).

Comparison Between the 2 VOIs. In the control group, the median BMD was significantly higher in the 250-μm versus the 4-mm VOI at the tibial midportion only ($P = .016$). In the DBM group, the median BMD was significantly higher in the 250-μm versus the 4-mm VOI at the femoral aperture ($P = .008$), femoral midportion ($P = .008$), femoral exit ($P = .008$), and tibial exit ($P = .032$). In the BMSC group, the median BMD was significantly higher in the 250-μm versus the 4-mm VOI at the femoral midportion ($P = .032$) and tibial midportion ($P = .016$). In the PRP group, the median BMD was significantly higher in the 250-μm versus the 4-mm VOI at the femoral midportion ($P = .016$), tibial aperture ($P = .016$), tibial midportion ($P = .008$), and tibial exit ($P = .032$).

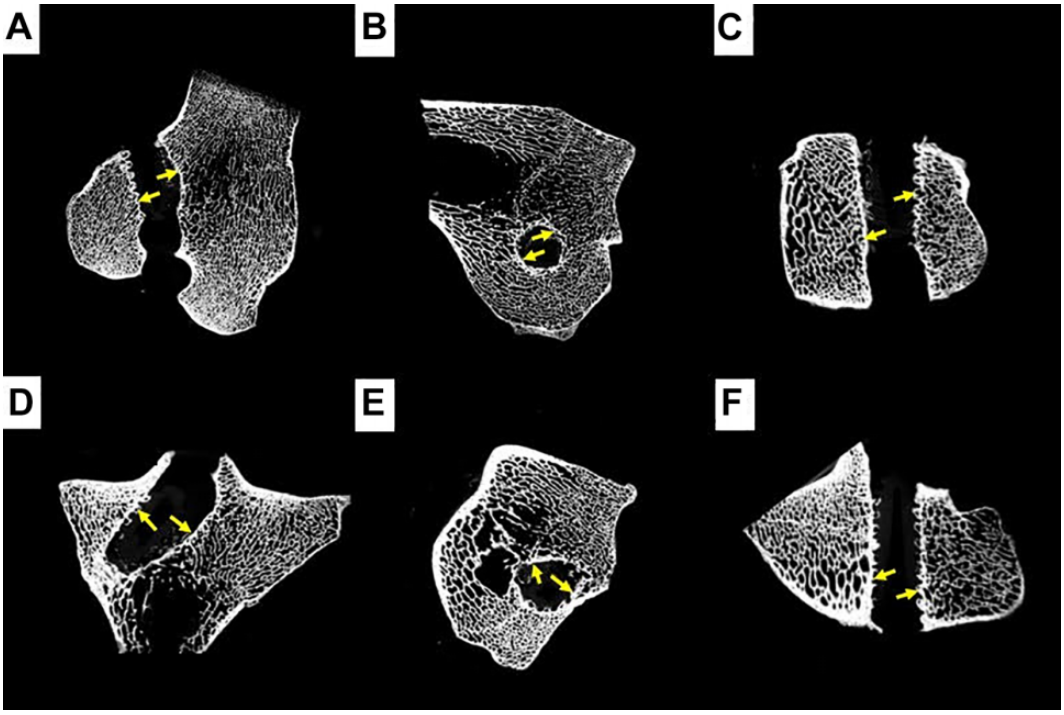

Figure 9. A representative image of femoral (A-C) and tibial (D-F) bone tunnels with sclerotic margins (yellow arrows). Femoral tunnel views: (A) coronal, (B) sagittal, and (C) transaxial views; tibial tunnel views: coronal (D), sagittal (E), and (F) transaxial views.

Tunnel Wall Sclerosis

Sclerotic margins were seen in the bone tunnels across all orientations (Figure 9). Sclerosis was seen in all 4 treatment groups. The most common site of sclerosis was the femoral aperture, where sclerosis was seen in all groups, whereas the least common site for sclerosis was the tibial aperture (Table 1). Sclerosis was most often seen in the control and BMSC groups (two-thirds of tunnel segments) and least commonly seen in the PRP group (one-third of tunnel segments). In the DBM group, sclerosis was seen in all femoral segments but not in any region of the tibia.

TABLE 1
Presence of Sclerosis by Treatment Group and Tunnel Segment[a]

Tunnel Segment	Control (n = 5)	DBM (n = 5)	BMSC (n = 5)	PRP (n = 5)
Femur				
Aperture	X	X	X	X
Midportion	X	X	X	—
Exit	—	X	—	—
Tibia				
Aperture	—	—	—	—
Midportion	X	—	X	—
Exit	X	—	X	X

[a]BMSC, bone marrow–derived mesenchymal stromal cell; BV/TV, bone volume/total volume; DBM, demineralized bone matrix; PRP, platelet-rich plasma; Tb.N, trabecular number; Tb.Sp, trabecular separation; Tb.Th, trabecular thickness; VOI, volume of interest. An X indicates that at least 2 of the following criteria were met: significantly increased BV/TV, Tb.Th, and Tb.N and reduced Tb.Sp in the 250-μm VOI relative to the 4-mm VOI. A dash indicates that the criteria for sclerosis were not met.

Tunnel Widening

The tunnel widening data are shown in Table A4. A mild degree of tunnel widening was seen in all tunnel segments across all treatment groups (Table 2). Therefore, the overall prevalence of tunnel widening was 100%, with no significant differences seen among treatment groups at the different tunnel segments (Figure 10, A and B). However, there were spatial differences in tunnel widening. In the control group, widening at the femoral tunnel aperture was significantly greater than that at the femoral tunnel midportion ($P = .034$). In the PRP group, widening at the tibial tunnel aperture was significantly less than that at the tibial tunnel midportion ($P = .034$). In the BMSC group, the amount of tunnel widening at the tibial aperture was significantly less than that at the femoral aperture ($P = .008$). At the mid-portion of the tibial tunnel, tunnel widening in the BMSC group was significantly less than the control group.

Relationship Between the Trabecular Bone Structure in the 250-μm VOI and Widening

Significant correlation was found between bone tunnel widening and markers for sclerosis of the tunnel wall in the femur using the 250-μm VOI. In the midportion of the femoral tunnel, BV/TV in the 250-μm VOI was positively

TABLE 2
Tunnel Widening Classification Between Treatment Groups[a]

	Tunnel Segment					
	Femur			Tibia		
Tunnel Widening Grade	Aperture	Middle	Exit	Aperture	Middle	Exit
Control						
None	0	0	0	0	0	0
Mild	0	0	0	0	0	0
Moderate	0	1 (20)	1 (20)	1 (20)	0	0
Severe	3 (60)	2 (40)	3 (60)	3 (60)	2 (40)	3 (60)
Very severe	2 (40)	2 (40)	1 (20)	1 (20)	3 (60)	2 (40)
DBM group						
None	0	0	0	0	0	0
Mild	0	0	0	0	1 (20)	0
Moderate	0	1 (20)	1 (20)	1 (20)	1 (20)	1 (20)
Severe	4 (80)	3 (60)	3 (60)	3 (60)	3 (60)	2 (40)
Very severe	1 (20)	1 (20)	1 (20)	1 (20)	0	2 (40)
BMSC group						
None	0	0	0	0	0	0
Mild	0	0	1 (20)	0	0	0
Moderate	0	2 (40)	1 (20)	3 (60)	1 (20)	2 (40)
Severe	5 (100)	2 (40)	3 (60)	2 (40)	4 (80)	3 (60)
Very severe	0	1 (20)	0	0	0	0
PRP group						
None	0	0	0	0	0	0
Mild	1 (20)	4 (80)	1 (20)	1 (20)	0	0
Moderate	2 (40)	0	2 (40)	2 (40)	0	0
Severe	1 (20)	0	1 (20)	2 (40)	2 (40)	4 (80)
Very severe	1 (20)	1 (20)	1 (20)	0	3 (60)	1 (20)

[a]Data are reported as n (%). BMSC, bone marrow–derived mesenchymal stromal cell; DBM, demineralized bone matrix; PRP, platelet-rich plasma.

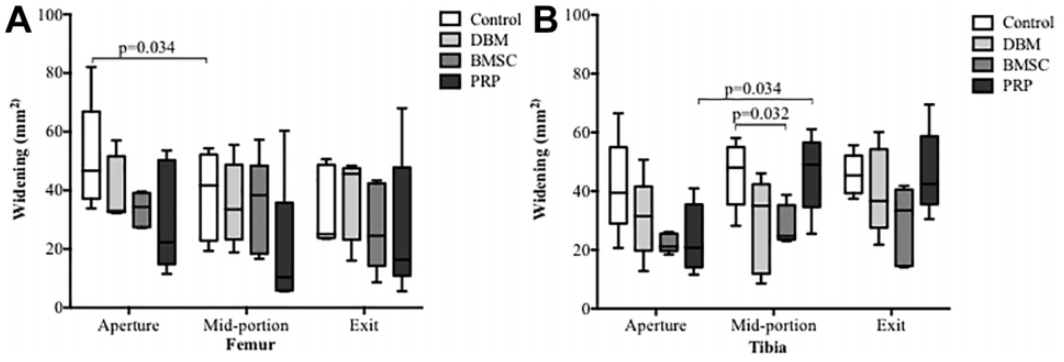

Figure 10. Box-and-whisker plots showing bone tunnel widening by treatment group in each bone tunnel. (A) Femur, (B) tibia (n = 5 for each group). BMSC, bone marrow–derived mesenchymal stromal cell; DBM, demineralized bone matrix; PRP, platelet-rich plasma.

correlated with tunnel widening ($r_S = 0.52$; $P = .019$) (Figure 11A). In the midportion of the femoral tunnel, Tb.N in the 250-μm VOI was positively correlated with tunnel widening ($r_S = 0.50$; $P = .024$) (Figure 11B) and exit ($r_S = 0.47$; $P = .038$) (Figure 11C). No significant correlations between trabecular bone analysis and bone tunnel widening were seen in the tibial tunnel (Table A5).

Radiographic Assessment of Bone Tunnel Appearance

The bone tunnels were clearly visible on plain radiographs after 12 weeks (Figure 12). Sclerotic tunnel walls were seen across all treatment groups and more often in the femoral tunnel than the tibial tunnel (Figure 12A).

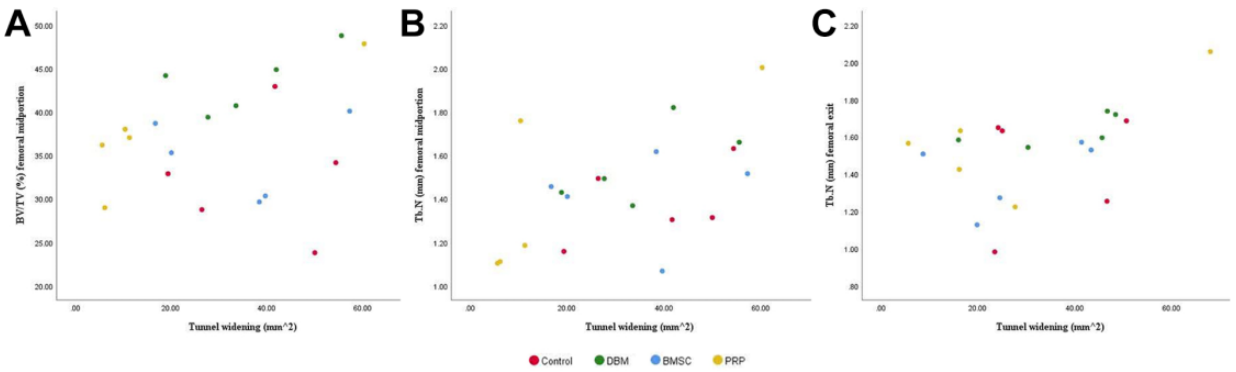

Figure 11. Scatter diagrams showing the relationship between (A) BV/TV in the 250-μm volume of interest (VOI) and bone tunnel widening in the midportion of the femoral tunnel ($r_S = 0.52$; $P = .019$), (B) Tb.N in the 250-μm VOI and bone tunnel widening in the midportion of the femoral tunnel ($r_S = 0.50$; $P = .024$), and (C) Tb.N in the 250-μm VOI and bone tunnel widening in the exit of the femoral tunnel ($r_S = 0.47$; $P = .038$). BMSC, bone marrow–derived mesenchymal stromal cell; BV/TV, bone volume/total volume; DBM, demineralized bone matrix; PRP, platelet-rich plasma; Tb.N, trabecular number.

Figure 12. Representative lateral radiograph showing the femoral bone tunnel (solid arrows) and tibial tunnel (dashed arrows) after 12 weeks. (A) control, (B) demineralized bone matrix, (C) bone marrow–derived mesenchymal stromal cell, and (D) platelet-rich plasma groups.

DISCUSSION

In this study, we investigated the effect of 3 orthobiologics (DBM, BMSCs, and PRP) on bone tunnel healing in a tendon allograft ACLR model. The clinical significance of bone formation at the tendon-bone interface is that it is correlated with mechanical pullout strength.[30] Overall, the greatest number of significant differences in the parameters measured occurred between the DBM and control groups. These differences were seen for BMD and BV/TV in the femoral tunnel, and widening at the aperture of the femoral tunnel was higher in the control group. Other

differences between groups were also seen, but these changes were less conclusive than were those seen between the DMB and control groups. We also found a significant correlation between bone sclerosis in the femoral tunnel midportion as measured using BV/TV and Tb.N and tunnel widening. Our hypothesis was only partly corroborated because no orthobiologic led to a significant reduction in bone tunnel widening.

Three small animal studies[13,16,19] have shown that DBM can enhance tendon-bone healing after ACLR as measured using histological analysis. Lovric et al[19] was the only study to use μCT analysis. For this analysis, 0.2 mL of human (xenogenic) DBM paste was applied to the flexor digitorum longus tendon autograft and bone tunnels in an immunodeficient rodent ACLR model. After 4 and 6 weeks, significantly higher BV/TV, Tb.Th, and BMD were observed in the DBM-treated group compared with the control group, which was correlated with increased woven bone formation and bone remodeling on histology.[13,16,19] In our study, we observed an effect with DBM in the femoral tunnel at the aperture and midportion in terms of BV/TV and BMD. The mechanism of action of DBM is likely to be due to increased osteoinductive growth factors such as bone morphogenic proteins at the interface,[27] and greater bone changes at the aperture might reflect the "packing" of material at the aperture after the graft was secured. When using DBM, we saw no significant differences in the tibia, which indicates that the bone tunnel (femoral vs tibial) influences the effect of DBM. A reason why DBM only showed an effect in the femur could be the anatomic differences between the 2 tunnels, with the tibia having less bone volume because of the medullary canal. The length of the femoral tunnel was shorter than was the femoral tunnel, and a second reason for differences between the femoral and tibial tunnel could be differences in the local biomechanical environment at the tendon-bone interface. Our study is the first preclinical study to determine the effect of DBM on bone tunnel widening and no significant effect on bone tunnel widening was seen with DBM treatment. Despite DBM stimulating greater bone responses, DBM-treated animals also experienced some of the greatest widening, and it is possible that some of the bone reaction was a response to the tunnel-widening process itself.

There is an expanding body of evidence that shows MSCs can enhance early tendon-bone healing in small animals, but relatively few studies have used μCT analysis.[12] In our study in the BMSC group, widening at the tibial aperture was significantly less than that at the femoral aperture. In a lapine study, Hur et al[14] applied 10 million BMSCs in fibrin glue to the ends of the extensor digitorum longus autograft and both bone tunnels and compared this with grafts receiving fibrin glue alone and an untreated control group. These authors reported that BMSCs led to reduction in tunnel widening in both femoral and tibial tunnels; however, no difference was seen between BMSCs and fibrin glue groups, so it is unclear if this effect was caused by the fibrin glue or BMSCs. No statistical difference was seen in BMD in this study, and trabecular bone analysis was not reported. Mifune et al[22] measured the BV/TV in the bone portion of the tibial tunnel 1 mm from the articular surface and observed that application of ACL-derived cells expressing Cluster of differentiation 34 (CD34+), isolated from remnant ACL tissues, enhanced perigraft bone mass compared with the untreated group after 4 weeks. Jang et al[15] reported that application of human (xenogenic) umbilical cord blood–derived mesenchymal stem cell reduced bone tunnel widening compared with an untreated control in both the femoral and the tibial bone tunnels when measured at a single location at a 5-mm depth from the tunnel aperture. The methodology used for μCT in this study was more comprehensive, which showed that BMSCs did not influence the trabecular bone analysis, BMD, or tunnel widening. Future research is required to determine the ultimate fate and mechanism of action of MSCs applied to the tendon-bone interface.

To the best of our knowledge, there have been no preclinical studies reporting the effect of PRP on bone tunnel healing using quantitative μCT analysis. In this study, PRP treatment appeared to have a beneficial effect at the tibial aperture, which was the site of least widening in the tibial tunnel and greatest BMD in the PRP-treated group. In a rabbit model, Teng et al[37] applied 0.1 mL of PRP immobilized in 0.1 mL of fibrin glue to semitendinosus autografts. After 8 weeks, greater bone formation was seen next to the bone tunnel using μCT, but the strength of the graft was not increased.[37] Zhai et al[47] did not report findings for PRP alone but showed that a combination of PRP and deproteinized bone enhanced early graft healing with reduced tunnel widening and increased BMD at 8 weeks. A small number of clinical studies have reported positive effects of PRP on differences between magnetic resonance imaging (MRI) and CT scans, but findings were not statistically significant and were not associated with improvements in clinical outcomes.[23,35,42] Starantzis et al[35] measured femoral tunnel widening using MRI and reported that PRP might have a beneficial effect on tunnel widening on MRI scans, although this was not statistically significant. Similarly, Mirzatolooei et al[23] measured tunnel widening using CT, and although there was a trend toward less widening in the PRP group, nonstatistically significant differences were observed. In this study, PRP did not seem to have a significant effect on bone tunnel healing compared with the control. However, in the tibial tunnel, there was less widening at the aperture compared with the midportion. This might be a result of the anatomy of the sheep tibia, which has a small distance of trabecular bone before the medullary canal.[21]

When evaluating bone tunnel widening, it is recommended that the bone tunnel diameter is measured perpendicular to the tunnel axis for at least 3 sites in the tunnel.[8] In this study, the bone tunnels were divided into thirds as described previously.[10,48] In our study, there were no significant differences between femoral and tibial tunnels in the control group for trabecular bone analysis or BMD. Nevertheless, some differences were seen when using orthobiologics. BMSC treatment was associated with increased Tb.Th in the femoral midportion and exit compared with the tibia, and in the PRP and DBM groups, there was increased BMD at the femoral exit compared with the tibial exit. One explanation for the differences seen between the femur and tibia is the different anatomy. In the femur, there is more cancellous bone surrounding the tunnel, whereas in the tibia, the

tunnel can merge with the medullary canal making it difficult to retain treatments applied to the tunnel wall. Variability in the local biomechanical environment may also play an important role in the observed differences between the femoral and tibial tunnels.

In the BMSC group, widening at the tibial aperture was significantly less than at the femoral aperture, which might be because the fibrin glue was less likely to be lost from the tibial tunnel, as the screw occupied a smaller proportion of the tunnel length when compared with that of the femur. Other studies[3,31,48] have demonstrated less bone formation at the aperture compared with other regions in the bone tunnel. Zong et al[48] showed statistically lower BMD and BV/TV at the femoral and tibial tunnel apertures. Bedi et al[3] was the first study to examine the differences in the tendon-bone healing process at different ends of the bone tunnel and observed differences as early as 1 week in their rodent model. Compared with the tunnel aperture, which was shown to have a greater number of osteoclasts, the tunnel exit was associated with superior collagen fiber continuity, orientation, and new bone formation.[3] In a rabbit model using suspensory fixation, graft-tunnel motion was greatest at the tunnel apertures with closer apposition of bone to tendon seen at the tunnel exits than at the tunnel aperture.[31] Ficek et al[10] reported the bone tunnel enlargement in sheep using suspensory fixation and Achilles tendon autograft. After 12 weeks, the tunnel tended to be wider at its aperture in the control group, whereas this was not seen in the group using a poly-96L/4D-lactic acid stent.[10]

In humans, MRI shows that tunnel widening occurs in the first 6 to 24 weeks,[44] but despite conflicting reports, a systematic review showed no significant difference in femoral tunnel widening between the aperture and midportion in humans.[5] Possible reasons why widening would be greater at the aperture compared with midportion include biological factors such as synovial fluid influx containing osteolytic cytokines[36] and increased graft tunnel motion.[31] In this study, the control group showed greater tunnel widening at the femoral aperture compared with the femoral midportion. However, in the treatment groups, this effect was not observed, which suggests that the orthobiologic treatments may have improved healing at the femoral aperture.

Tunnel wall sclerosis after ACLR is a recognized phenomenon.[2] In this study, sclerosis was seen in all treatment groups, and it was more common in the femoral tunnel, especially at the femoral aperture. Currently, the mechanism for sclerosis is unknown, and its clinical significance is uncertain. Neddermann et al[24] first described an association between tunnel widening and sclerosis of the tunnel wall in the femoral tunnels of sheep. The differences between that study and ours are that we used older sheep (age, 2-3 years vs 4 months) and an interference screw fixation system compared with Endobutton (femur) and suture washer (tibial fixation). Our study investigated both the femoral and the tibial tunnels. On radiographs in our study, sclerosis of the tunnel walls was more commonly seen in the control group, and both Tb.N and BV/TV were significantly correlated with femoral tunnel widening. Hence, this study suggests the link between widening and sclerosis only holds true for the femoral tunnel and does not apply to the whole tunnel. Future research is needed that correlates μCT findings with histological appearances, which would delineate if sclerosis is associated with favorable or negative tendon-bone healing and clinical outcomes.

Various factors may account for bone tunnel widening, including both biological and biomechanical considerations. Biological factors may include local bone necrosis from drilling, immune response to the allograft tendon, and the presence of catabolic and inflammatory cytokines in the postsurgical joint. The biomechanical environment at the graft-bone interface will also affect the local biological events, with increased graft-tunnel motion at the aperture postulated to play a role.[46] A major weakness in our animal model was that we used an outside-in screw insertion technique, which might have had lower stiffness compared with true "aperture" fixation and contributed to greater graft-tunnel motion at the apertures.

Strengths and Limitations

To our knowledge, this is the first large animal study using contemporary fixation methods comparing μCT findings for bone adjacent to ACL bone tunnels that have been treated with orthobiologics. A strength of this study is the comprehensive analysis of both femoral and tibial tunnels, along with an analysis of segments to clarify spatial changes to examine tunnel sclerosis.

Nevertheless, this preclinical sheep model has significant limitations, and the results of an ovine model cannot be directly extrapolated to the human clinical situation. First, there are differences in BMD between humans and sheep,[1] with the sheep tibia having only a small amount of cancellous bone between the joint surface and the medullary canal, especially in the tibia. This is significant because BMD affects soft tissue graft fixation.[26] Second, as our sheep were freely weightbearing, it was not possible to control the effects of mechanical loading in this sheep model.[20,34] Another limitation is that full characterization of the PRP and BMSCs was not fully reported and did not fulfill recently published reporting standards.[6,28] In addition, analysis was conducted at only 1 time point, and tunnel widening may continue to develop over a longer period.[4,41] A superior study design would include multiple time points of analysis, including earlier and later time points, which would allow changes to be tracked over time. The 12-week time point for analysis was specifically chosen because animal studies have indicated that pullout of the tendon graft from the bone tunnel can occur up to this point.[11,25,39] The relatively small number of animals per group may have resulted in type II error.

It is also possible that orthobiologics might have had a beneficial effect at the tendon-bone interface that was not detected on μCT. For instance, regeneration of a morphologically superior "direct-type" insertion better resembling the ACL insertion may have occurred. Furthermore, the effect of the biologic treatments on the biomechanical properties of the graft, such as pullout strength, was not examined. Hence, determining the effect of orthobiologics on biomechanical and histological outcomes, including at the collagen fibril level, represents an important area for future

research and would provide an insight into the association between imaging and histological outcomes. Finally, to elucidate the effects of fibrin glue more clearly, a better study design would have included an additional group in which applied fibrin glue was applied without MSCs.

CONCLUSION

Bone healing in ACL femoral bone tunnels in a tendon allograft ACLR model was most enhanced by DBM. No orthobiologic treatment led to a reduction in bone tunnel widening. Sclerosis of the tunnel wall was common across all groups and correlated with tunnel widening in the midportion of the femoral tunnel.

ACKNOWLEDGMENT

The authors acknowledge Mark Hopkinson, departmental technician from the Royal Veterinary College, who helped optimize the technique for μCT interpretation.

REFERENCES

1. Aerssens J, Boonen S, Lowet G, Dequeker J. Interspecies differences in bone composition, density, and quality: potential implications for in vivo bone research. *Endocrinology*. 1998;139(2):663-670.
2. Akoto R, Müller-Hübenthal J, Balke M, et al. Press-fit fixation using autologous bone in the tibial canal causes less enlargement of bone tunnel diameter in ACL reconstruction—a CT scan analysis three months postoperatively. *BMC Musculoskelet Disord*. 2015;16(1):200.
3. Bedi A, Kawamura S, Ying L, Rodeo SA. Differences in tendon graft healing between the intra-articular and extra-articular ends of a bone tunnel. *HSS J*. 2009;5(1):51-57.
4. Buelow J-U, Siebold R, Ellermann A. A prospective evaluation of tunnel enlargement in anterior cruciate ligament reconstruction with hamstrings: extracortical versus anatomical fixation. *Knee Surg Sports Traumatol Arthrosc*. 2002;10(2):80-85.
5. Celik H, Lee D-H. Comparison of the aperture and midportion femoral tunnel widening after anterior cruciate ligament reconstruction: a systematic review and meta-analyses. *Medicine*. 2019;98(26):e16121.
6. Chahla J, Cinque ME, Piuzzi NS, et al. A call for standardization in platelet-rich plasma preparation protocols and composition reporting: a systematic review of the clinical orthopaedic literature. *J Bone Joint Surg Am*. 2017;99(20):1769-1779.
7. Davey MS, Hurley ET, Withers D, Moran R, Moran CJ. Anterior cruciate ligament reconstruction with platelet-rich plasma: a systematic review of randomized control trials. *Arthroscopy*. 2020;36(4):1204-1210.
8. de Beus A, Koch JE, Hirschmann A, Hirschmann MT. How to evaluate bone tunnel widening after ACL reconstruction—a critical review. *Muscles Ligaments Tendons J*. 2017;7(2):230.
9. Derwin KA, Galatz LM, Ratcliffe A, Thomopoulos S. Enthesis repair: challenges and opportunities for effective tendon-to-bone healing. *J Bone Joint Surg Am*. 2018;100(16):e109.
10. Ficek K, Rajca J, Stolarz M, et al. Bioresorbable stent in anterior cruciate ligament reconstruction. *Polymers (Basel)*. 2019;11(12):1961.
11. Goradia VK, Rochat MC, Grana WA, Rohrer MD, Prasad HS. Tendon-to-bone healing of a semitendinosus tendon autograft used for ACL reconstruction in a sheep model. *Am J Knee Surg*. 2000;13(3):143-151.
12. Guo R, Gao L, Xu B. Current evidence of adult stem cells to enhance anterior cruciate ligament treatment: a systematic review of animal trials. *Arthroscopy*. 2018;34(1):331-340.e332.
13. Hsu SL, Wang CJ. The use of demineralized bone matrix for anterior cruciate ligament reconstruction: a radiographic, histologic, and immunohistochemical study in rabbits. *J Surg Res*. 2014;187(1):219-224.
14. Hur C-I, Ahn H-W, Seon J-K, Song E-K, Kim G-E. Mesenchymal stem cells decrease tunnel widening of anterior cruciate ligament reconstruction in rabbit model. *Int J Stem Cells*. 2019;12(1):162-169.
15. Jang K-M, Lim HC, Jung WY, Moon SW, Wang JH. Efficacy and safety of human umbilical cord blood–derived mesenchymal stem cells in anterior cruciate ligament reconstruction of a rabbit model: new strategy to enhance tendon graft healing. *Arthroscopy*. 2015;31(8):1530-1539.
16. Kiliçoğlu Ö, Dikmen G, Koyuncu Ö, Bilgic B, Alturfan AK. Effects of demineralized bone matrix on tendon-bone healing: an in vivo, experimental study on rabbits. *Acta Orthop Traumatol Turc*. 2012;46(6):443-448.
17. Kondo E, Yasuda K, Katsura T, Hayashi R, Azuma C, Tohyama H. Local administration of autologous synovium-derived cells improve the structural properties of anterior cruciate ligament autograft reconstruction in sheep. *Am J Sports Med*. 2011;39(5):999-1007.
18. Kondo E, Yasuda K, Katsura T, Hayashi R, Kotani Y, Tohyama H. Biomechanical and histological evaluations of the doubled semitendinosus tendon autograft after anterior cruciate ligament reconstruction in sheep. *Am J Sports Med*. 2012;40(2):315-324.
19. Lovric V, Chen D, Yu Y, Oliver RA, Genin F, Walsh WR. Effects of demineralized bone matrix on tendon-bone healing in an intra-articular rodent model. *Am J Sports Med*. 2012;40(10):2365-2374.
20. Ma R, Schar M, Chen T, et al. Effect of dynamic changes in anterior cruciate ligament in situ graft force on the biological healing response of the graft-tunnel interface. *Am J Sports Med*. 2018;46(4):915-923.
21. Magen HE, Howell SM, Hull ML. Structural properties of six tibial fixation methods for anterior cruciate ligament soft tissue grafts. *Am J Sports Med*. 1999;27(1):35-43.
22. Mifune Y, Matsumoto T, Ota S, et al. Therapeutic potential of anterior cruciate ligament-derived stem cells for anterior cruciate ligament reconstruction. *Cell Transplant*. 2012;21(8):1651-1665.
23. Mirzatolooei F, Alamdari M, Khalkhali H. The impact of platelet-rich plasma on the prevention of tunnel widening in anterior cruciate ligament reconstruction using quadrupled autologous hamstring tendon: a randomised clinical trial. *Bone Joint J*. 2013;95(1):65-69.
24. Neddermann A, Willbold E, Witte F, et al. Tunnel widening after anterior cruciate ligament reconstruction: an experimental study in sheep. *Am J Sports Med*. 2009;37(8):1609-1617.
25. Park M, Lee MC, Seong S. A comparative study of the healing of tendon autograft and tendon-bone autograft using patellar tendon in rabbits. *Int Orthop*. 2001;25(1):35-39.
26. Pena F, Grontvedt T, Brown GA, Aune AK, Engebretsen L. Comparison of failure strength between metallic and absorbable interference screws: influence of insertion torque, tunnel-bone block gap, bone mineral density, and interference. *Am J Sports Med*. 1996;24(3):329-334.
27. Pietrzak WS, Dow M, Gomez J, Soulvie M, Tsiagalis G. The in vitro elution of BMP-7 from demineralized bone matrix. *Cell Tissue Bank*. 2012;13(4):653-661.
28. Piuzzi NS, Hussain ZB, Chahla J, et al. Variability in the preparation, reporting, and use of bone marrow aspirate concentrate in musculoskeletal disorders: a systematic review of the clinical orthopaedic literature. *J Bone Joint Surg Am*. 2018;100(6):517-525.
29. Rodeo S. Cell therapy in orthopaedics: where are we in 2019? *Bone Joint J*. 2019;101(4):361-364.
30. Rodeo SA, Arnoczky SP, Torzilli PA, Hidaka C, Warren RF. Tendon-healing in a bone tunnel: a biomechanical and histological study in the dog. *J Bone Joint Surg Am*. 1993;75(12):1795-1803.
31. Rodeo SA, Kawamura S, Kim H-J, Dynybil C, Ying L. Tendon healing in a bone tunnel differs at the tunnel entrance versus the tunnel exit: an effect of graft-tunnel motion? *Am J Sports Med*. 2006;34(11):1790-1800.
32. Sánchez M, Anitua E, Azofra J, Prado R, Muruzabal F, Andia I. Ligamentization of tendon grafts treated with an endogenous preparation rich in growth factors: gross morphology and histology. *Arthroscopy*. 2010;26(4):470-480.
33. Sánchez M, Anitua E, Delgado D, et al. Ultrasound-guided plasma rich in growth factors injections and scaffolds hasten motor nerve functional recovery in an ovine model of nerve crush injury. *J Tissue Eng Regenerat Med*. 2017;11(5):1619-1629.

34. Song F, Jiang D, Wang T, et al. Mechanical loading improves tendon-bone healing in a rabbit anterior cruciate ligament reconstruction model by promoting proliferation and matrix formation of mesenchymal stem cells and tendon cells. *Cell Physiol Biochem*. 2017;41(3):875-889.
35. Starantzis KA, Mastrokalos D, Koulalis D, Papakonstantinou O, Soucacos PN, Papagelopoulos PJ. The potentially positive role of PRPs in preventing femoral tunnel widening in ACL reconstruction surgery using hamstrings: a clinical study in 51 patients. *J Sports Med (Hindawi Publ Corp)*. 2014;2014:789317.
36. Sun L, Zhou X, Wu B, Tian M. Inhibitory effect of synovial fluid on tendon-to-bone healing: an experimental study in rabbits. *Arthroscopy*. 2012;28(9):1297-1305.
37. Teng C, Zhou C, Xu D, Bi F. Combination of platelet-rich plasma and bone marrow mesenchymal stem cells enhances tendon–bone healing in a rabbit model of anterior cruciate ligament reconstruction. *J Orthop Surg Res*. 2016;11(1):96.
38. Tisherman R, Wilson K, Horvath A, Byrne K, De Groot J, Musahl V. Allograft for knee ligament surgery: an American perspective. *Knee Surg Sports Traumatol Arthrosc*. 2019;27(6):1882-1890.
39. Tomita F, Yasuda K, Mikami S, Sakai T, Yamazaki S, Tohyama H. Comparisons of intraosseous graft healing between the doubled flexor tendon graft and the bone–patellar tendon–bone graft in anterior cruciate ligament reconstruction. *Arthroscopy*. 2001;17(5):461-476.
40. Urist MR. Bone: formation by autoinduction. *Science*. 1965; 150(3698):893-899.
41. Vadalà A, Iorio R, De Carli A, et al. The effect of accelerated, brace free, rehabilitation on bone tunnel enlargement after ACL reconstruction using hamstring tendons: a CT study. *Knee Surg Sports Traumatol Arthrosc*. 2007;15(4):365-371.
42. Ventura A, Terzaghi C, Borgo E, Verdoia C, Gallazzi M, Failoni S. Use of growth factors in ACL surgery: preliminary study. *J Orthop Traumatol*. 2005;6(2):76-79.
43. Vermeijden HD, Yang XA, van der List JP, DiFelice GS, Rademakers MV, Kerkhoffs G. Trauma and femoral tunnel position are the most common failure modes of anterior cruciate ligament reconstruction: a systematic review. *Knee Surg Sports Traumatol Arthrosc*. 2020; 28(11):3666-3675.
44. Weber AE, Delos D, Oltean HN, et al. Tibial and femoral tunnel changes after ACL reconstruction: a prospective 2-year longitudinal MRI study. *Am J Sports Med*. 2015;43(5):1147-1156.
45. Yoshikawa T, Tohyama H, Katsura T, et al. Effects of local administration of vascular endothelial growth factor on mechanical characteristics of the semitendinosus tendon graft after anterior cruciate ligament reconstruction in sheep. *Am J Sports Med*. 2006;34(12):1918-1925.
46. Yue L, DeFroda SF, Sullivan K, Garcia D, Owens BD. Mechanisms of bone tunnel enlargement following anterior cruciate ligament reconstruction. *JBJS Rev*. 2020;8(4):e0120.
47. Zhai W, Lv C, Zheng Y, Gao Y, Ding Z, Chen Z. Weak link of tendon–bone healing and a control experiment to promote healing. *Arch Orthop Trauma Surg*. 2013;133(11):1533-1541.
48. Zong JC, Ma R, Wang H, et al. The effect of graft pretensioning on bone tunnel diameter and bone formation after anterior cruciate ligament reconstruction in a rat model: evaluation with micro-computed tomography. *Am J Sports Med*. 2017;45(6):1349-1358.

APPENDIX

TABLE A1
Trabecular Bone Analysis of 4-mm VOI[a]

	Femoral Tunnel				Tibial Tunnel			
Parameter	DBM	BMSC	PRP	Control	DBM	BMSC	PRP	Control
Tunnel aperture								
BV/TV, %	52.7 (48.4-64.6)	43.8 (33.8-46.8)	44.9 (39.5-48.8)	31.8 (20.5-45.2)	46.2 (41.6-59.5)	46.7 (39.1-54.0)	40.2 (37.4-46.7)	40.94 (37.0-43.7)
Tb.Th, mm	0.41 (0.38-0.42)	0.35 (0.30-0.37)	0.36 (0.36-0.40)	0.36 (0.29-0.38)	0.41 (0.40-0.49)	0.49 (0.46-0.51)	0.40 (0.37-0.52)	0.36 (0.32-0.48)
Tb.Sp, mm	0.58 (0.49-0.60)	0.57 (0.55-0.62)	0.62 (0.57-0.74)	0.59 (0.56-0.65)	0.64 (0.54-0.70)	0.69 (0.62-0.80)	0.73 (0.60-0.88)	0.66 (0.62-0.75)
Tb.N, 1/mm	1.38 (1.18-1.50)	1.21 (1.14-1.28)	1.17 (1.10-1.25)	0.98 (0.70-1.19)	1.09 (1.04-1.23)	0.95 (0.85-1.05)	0.92 (0.89-1.08)	1.07 (0.91-1.20)
Tunnel midportion								
BV/TV, %	44.2 (40.1-46.8)	35.3 (30.0-39.4)	37.1 (32.6-42.9)	32.9 (26.3-38.6)	44.3 (36.7-52.6)	39.4 (36.8-44.4)	38.1 (28.1-41.5)	32.6 (28.5-37.3)
Tb.Th, mm	0.33 (0.33-0.39)	0.31 (0.28-0.32)	0.31 (0.28-0.39)	0.29 (0.25-0.41)	0.40 (0.36-0.43)	0.39 (0.35-0.47)	0.36 (0.29-0.37)	0.33 (0.31-0.38)
Tb.Sp, mm	0.61 (0.55-0.62)	0.63 (0.59-0.67)	0.66 (0.59-0.70)	0.65 (0.64-0.69)	0.63 (0.57-0.71)	0.72 (0.66-0.74)	0.73 (0.61-0.85)	0.76 (0.65-0.82)
Tb.N, 1/mm	1.20 (1.13-1.34)	1.17 (1.06-1.25)	1.12 (1.08-1.24)	1.10 (0.91-1.14)	1.11 (1.03-1.21)	1.02 (0.95-1.07)	1.06 (0.96-1.11)	0.97 (0.89-1.03)
Tunnel exit								
BV/TV, %	44.5 (40.3-48.7)	40.4 (35.9-46.8)	42.4 (37.5-54.5)	38.7 (18.1-45.2)	46.4 (39.2-51.2)	46.86 (42.9-48.5)	45.3 (42.4-48.2)	34.0 (32.3-44.8)
Tb.Th, mm	0.36 (0.34-0.45)	0.33 (0.32-0.38)	0.34 (0.31-0.46)	0.33 (0.24- 0.42)	0.45 (0.34-0.48)	0.41 (0.39-0.50)	0.44 (0.38-0.47)	0.36 (0.33-0.47)
Tb.Sp, mm	0.58 (0.53-0.60)	0.60 (0.53-0.67)	0.61 (0.52-0.64)	0.72 (0.57-1.2)	0.59 (0.47-0.77)	0.65 (0.63-0.67)	0.69 (0.58-0.78)	0.79 (0.64-0.81)
Tb.N, 1/mm	1.22 (1.14-1.32)	1.24 (1.02-1.26)	1.20 (1.13-1.26)	0.95 (0.76-1.24)	1.16 (0.89-1.33)	1.08 (0.97-1.13)	1.03 (1.01-1.14)	0.94 (0.93-1.02)

[a]Data are reported as median (interquartile range). BV/TV, bone volume/total volume; DBM, demineralized bone matrix; BMSC, bone marrow–derived mesenchymal stromal cells; PRP platelet-rich plasma; Tb.N, trabecular number; Tb.Sp, trabecular separation; Tb.Th, trabecular thickness; VOI, volume of interest.

TABLE A2
Trabecular Bone Analysis of 250-μm VOI[a]

	Femoral Tunnel				Tibial Tunnel			
Parameter	DBM	BMSC	PRP	Control	DBM	BMSC	PRP	Control
Tunnel aperture								
BV/TV, %	66.9 (60.5-72.0)	60.9 (49.9-66.2)	44.2 (30.5-58.1)	62.5 (55.8-66.3)	48.2 (45.1-63.5)	62.8 (47.1-65.2)	50.4 (40.2-57.4)	53.1 (43.3-58.9)
Tb.Th, mm	0.41 (0.40-0.43)	0.39 (0.35-0.43)	0.34 (0.33-0.35)	0.41 (0.36-0.41)	0.44 (0.40-0.49)	0.48 (0.42-0.50)	0.36 (0.34-0.42)	0.39 (0.37-0.48)
Tb.Sp, mm	0.32 (0.28-0.42)	0.33 (0.30-0.39)	0.43 (0.34-0.46)	0.34 (0.31-0.42)	0.45 (0.38-0.75)	0.42 (0.37-0.65)	0.55 (0.33-0.87)	0.65 (0.38-0.81)
Tb.N, 1/mm	1.63 (1.43-1.74)	1.46 (1.41-1.58)	1.25 (0.91-1.75)	1.59 (1.51-1.62)	1.21 (1.00-1.43)	1.29 (1.09-1.35)	1.39 (1.03-1.54)	1.15 (1.13-1.36)
Tunnel midportion								
BV/TV, %	53.8 (52.5-61.1)	53.5 (42.8-54.8)	37.3 (35.1-59.8)	49.8 (40.1-52.2)	57.6 (46.9-62.3)	59.6 (51.6-64.6)	46.4 (32.7-55.1)	47.8 (41.5-53.2)
Tb.Th, mm	0.36 (0.35-0.38)	0.36 (0.33-0.37)	0.30 (0.26-0.33)	0.33 (0.32-0.37)	0.40 (0.39-0.47)	0.43 (0.39-0.45)	0.33 (0.31-0.39)	0.39 (0.36-0.46)
Tb.Sp, mm	0.37 (0.31-0.56)	0.41 (0.36-0.62)	0.66 (0.24-0.79)	0.57 (0.40-0.75)	0.40 (0.34-0.52)	0.34 (0.31-0.44)	0.39 (0.35-0.83)	0.46 (0.38-0.83)
Tb.N, 1/mm	1.49 (1.40-1.74)	1.46 (1.24-1.46)	1.19 (1.11-1.88)	1.31 (1.23-1.56)	1.31 (1.20-1.41)	1.40 (1.24-1.52)	1.31 (1.05-1.47)	1.28 (0.90-1.43)
Tunnel exit								
BV/TV, %	63.6 (60.8-67.8)	52.1 (37.7-56.6)	52.0 (44.4-63.0)	47.2 (40.9-53.7)	59.0 (50.4-63.8)	61.5 (56.6-62.5)	62.2 (48.1-72.9)	61.5 (45.8-65.5)
Tb.Th, mm	0.39 (0.37-0.41)	0.35 (0.31-0.37)	0.33 (0.32-0.36)	0.36 (0.28-0.38)	0.39 (0.38-0.45)	0.45 (0.40-0.47)	0.42 (0.38-0.47)	0.41 (0.36-0.51)
Tb.Sp, mm	0.31 (0.29-0.32)	0.39 (0.35-0.76)	0.37 (0.36-0.60)	0.35 (0.34-0.53)	0.33 (0.25-0.49)	0.40 (0.35-0.52)	0.36 (0.28-0.42)	0.36 (0.35-0.44)
Tb.N, 1/mm	1.60 (1.56-1.73)	1.51 (1.20-1.55)	1.57 (1.32-1.85)	1.63 (1.12-1.67)	1.50 (1.13-1.67)	1.30 (1.24-1.49)	1.47 (1.39-1.60)	1.28 (1.13-1.55)

[a]Data are reported as median (interquartile range). BV/TV, bone volume/total volume; DBM, demineralized bone matrix; BMSC, bone marrow–derived mesenchymal stromal cells; PRP platelet-rich plasma; Tb.N, trabecular number; Tb.Th, trabecular thickness; Tb.Sp, trabecular separation; VOI, volume of interest.

TABLE A3
BMD Data (in g/cm^2)[a]

	Femoral Tunnel				Tibial Tunnel			
Parameter	DBM	BMSC	PRP	Control	DBM	BMSC	PRP	Control
4-mm VOI								
Aperture	0.55 (0.53-0.57)	0.38 (0.31-0.51)	0.53 (0.47-0.63)	0.47 (0.28-0.50)	0.50 (0.42-0.60)	0.49 (0.36-0.57)	0.40 (0.39-0.48)	0.36 (0.28-0.47)
Midportion	0.44 (0.43-0.47)	0.35 (0.30-0.46)	0.43 (0.32-0.49)	0.30 (0.23-0.39)	0.39 (0.34-0.54)	0.35 (0.31-0.44)	0.34 (0.26-0.36)	0.24 (0.20-0.42)
Exit	0.44 (0.41-0.46)	0.44 (0.32-0.51)	0.48 (0.44-0.52)	0.39 (0.19-0.47)	0.37 (0.34-0.39)	0.33 (0.25-0.44)	0.21 (0.20-0.38)	0.24 (0.17-0.41)
250-μm VOI								
Aperture	0.73 (0.62-0.80)	0.57 (0.49-0.72)	0.74 (0.56-0.85)	0.65 (0.47-0.82)	0.63 (0.57-0.67)	0.60 (0.49-0.72)	0.74 (0.62-0.77)	0.57 (0.42-0.76)
Midportion	0.62 (0.58-0.68)	0.56 (0.46-0.77)	0.67 (0.54-0.73)	0.53 (0.35-0.80)	0.66 (0.52-0.71)	0.55 (0.48-0.67)	0.65 (0.45-0.71)	0.56 (0.44-0.58)
Exit	0.64 (0.59-0.74)	0.62 (0.51-0.68)	0.71 (0.57-0.73)	0.69 (0.39-0.73)	0.47 (0.40-0.64)	0.53 (0.39-0.56)	0.44 (0.38-0.49)	0.53 (0.35-0.60)

[a]Data are reported as median (interquartile range). BMD, bone mineral density; DBM, demineralized bone matrix; BMSC, bone marrow–derived mesenchymal stromal cells; PRP platelet-rich plasma; VOI, volume of interest.

TABLE A4
Tunnel Widening Data (in mm^2)[a]

Tunnel Segment	Control	DBM	BMSC	PRP
Femur				
Aperture	46.7 (37.1-66.9)	33.0 (32.6-51.6)	34.4 (27.5-39.1)	22.3 (14.9-50.3)
Midportion	41.7 (22.9-52.2)	33.5 (23.3-48.7)	38.4 (18.4-48.4)	10.4 (5.92-35.8)
Exit	25.1 (23.9-48.7)	45.6 (23.2-47.6)	24.6 (14.3-42.4)	16.4 (10.9-47.8)
Tibia				
Aperture	39.4 (29.0-55.0)	31.5 (19.7-41.6)	21.2 (19.7-25.5)	20.8 (14.1-35.5)
Midportion	48.0 (35.5-55.0)	35.1 (11.9-42.3)	24.7 (23.5-35.2)	49.1 (34.6-56.6)
Exit	45.3 (39.3-52.1)	36.6 (27.5-54.3)	33.4 (14.5-40.4)	42.4 (35.6-53.7)

[a]Data are reported as median (interquartile range). BMSC, bone marrow–derived mesenchymal stromal cells; DBM, demineralized bone matrix; PRP platelet-rich plasma.

TABLE A5
Spearman Correlation Coefficients of Tunnel Widening and Trabecular Bone Analysis for 250-μm VOI[a]

	BV/TV		Tb.Th		Tb.N		Tb.Sp	
Tunnel Segment	r_S	*P*	r_S	*P*	r_S	*P*	r_S	*P*
Femur								
Aperture	0.289	.217	0.012	.960	0.355	.125	–0.230	.329
Midportion	0.520	**.019**	–0.023	.925	0.504	**.024**	–0.371	.107
Exit	0.268	.254	–0.168	.478	0.468	**.038**	–0.444	.050
Tibia								
Aperture	0.137	.565	–0.171	.471	0.328	.158	–0.057	.810
Midportion	–0.158	.506	–0.002	.995	0.050	.835	0.030	.900
Exit	–0.199	.400	–0.426	.061	–0.042	.860	–0.087	.715

[a]Significant values are in bold. BV/TV, bone volume/total volume; Tb.N, trabecular number; Tb.Sp, trabecular separation; Tb.Th, trabecular thickness; VOI, volume of interest.